Hierarchical block model for earthquakes

Sergiy V. Mykulyak*
Institute of Geophysics, NASU, Kiev 03680, Ukraine

(Received 24 October 2017; revised manuscript received 22 May 2018; published 18 June 2018)

The presented model for earthquakes is based on two fundamental principles: the hierarchical structure of seismic areas and the concept of self-organized criticality. The model reproduces the basic empirical properties of seismic processes: the frequency-energy scaling relation (the Gutenberg-Richter law), the generalized Omori law for temporal decay of aftershocks, the aftershock productivity law, the fractal distributions of hypocenters (epicenters) with power-law dependencies of the number of events on distances between hypocenters (epicenters), and, finally, the γ distribution for waiting times. In the model, the threshold energies depend on the block sizes and are distributed according to the Gauss law. After strong earthquakes they are redistributed at the decreasing average values. The change of threshold energies leads to the triggering of aftershock series.

DOI: 10.1103/PhysRevE.97.062130

Earth's lithosphere is a substantially inhomogeneous medium possessing hierarchical structure [1,2]. It consists of tectonic blocks separated by a network of faults and forming a multilevel system of volumes (blocks). This hierarchy covers scales from thousands of kilometers (tectonic plates) to millimeters (granules in rocks) and is most brightly manifested at the tectonic plate boundaries [2–4]. The kinetic energy of moving tectonic plates is supplied continuously to boundary areas and is redistributed among the hierarchy. Part of this energy is dissipated and another part is transformed into elastic energy, which is released eventually as earthquakes. A number of empirical regularities have been established for seismic processes, which are characterized by large-scale invariance: the Gutenberg-Richter (GR) law, which relates the number of earthquakes to their magnitudes [5], the Omori law, which describes the attenuation of aftershocks [6–10], the Utsu aftershock productivity law expressing the total number of aftershocks generated by a mainshock [8,9], and the fractal distributions of hypocenters and power-law distributions for epicenters indicating a fractal distribution of earthquakes in space [11–15]. Earthquakes also demonstrate a long-range space-time correlation and clustering [16–24]. The crackling noise generated by porous materials, woods, charcoal samples, volcanic rocks, magnetics, etc. has the same properties [25–29].

Hierarchical structuring, the exchange of energy with the external environment, and the lack of scale in seismic processes lead to the need to consider the seismic zone as an open complex hierarchical system, and the large-scale invariance of seismic processes indicates that the system is in the critical state. Bak *et al.* [30,31] simulated the behavior of a pile of sand as a system in critical condition that makes self-adjustments to remain permanently in that state. They called this state of the system self-organized criticality (SOC). The SOC concept for earthquake modeling was carried out by a number of authors [32–36]. Most of these models are based on the spring-block model by Burridge and Knopoff [37]. Rundle, Jackson, and Brown (RJB) [38,39] modified this model into a cellular automation model that was then transformed into a lattice form by Olami, Feder, and Cristensen (OFC) [34]. The rest of the SOC models were originally built on the basis of cellular automata [32,40–42].

Traditional SOC models have been modified and refined to describe better both GR scaling and the spatiotemporal correlations of earthquakes that are expressed in the existence of foreshocks and aftershocks, as well as in their fractal distribution. Ito and Matsuzaki [33] modified the cellular automation model with a simple procedure of redistributing forces after each earthquake. This led to the fact that any earthquake could trigger aftershocks. The more complex mechanism for the distribution of tectonic stresses on a fault leading to long-range correlations has been offered in the Baiesi model [43]. In some RJB and OFC models spatiotemporal correlations in the seismic process are achieved by introducing the corresponding inhomogeneities. The simplest heterogeneities have been introduced as point or line defects [44–46]. Serino *et al.* [47] complicated the model, considering the fault system with different levels of defects instead of a single fault system, and Dominguez *et al.* [48] added damaged cells that do not hold stress but dissipate energy. Kazemian *et al.* [49] introduced stronger sites or asperity cells to the lattice. These structured asperities reproduce the clustering of foreshocks and aftershocks well. In the fault system models [47,49], long-range stress transfer from critical sites, where the critical force is exceeded, is used. Another kind of heterogeneity, used in the advanced RJB and OFC models, is the random distribution of stress thresholds controlling block stability [50,51]. In order to reproduce the processes of spatiotemporal earthquake clustering, Jagla [51] included the mechanism of structural relaxation in the OFC model.

All the cells in standard cellular automation models have the same size and all the blocks in the spring-block models are similar as well. Barriere and Turcotte [40,41] and Huang [42] *et al.* learned the cellular automation SOC model defined on a hierarchically constructed grid with a fractal distribution of cell sizes. However, in these models, the partition of the grid into cells is regular.

*mykulyak@ukr.net

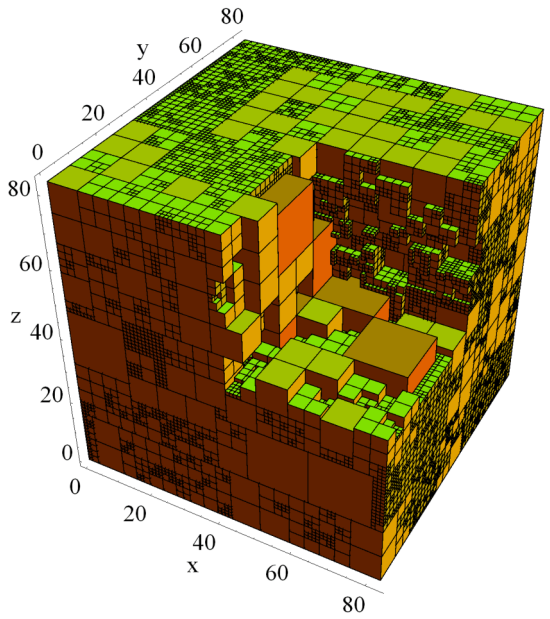

FIG. 1. The seismic area Ω as a hierarchical block system.

The model proposed in this paper takes into account the hierarchical structure of the seismic zone and the fact that it is in a state of self-organized criticality. The seismic area Ω in the form of a cube is formed by a hierarchical system of cubic blocks arranged in a random order (Fig. 1). It does not solve a specific boundary problem, but the possibility of modeling a natural seismic process using the hierarchical block model is studied. Energy enters the system from outside and accumulates unevenly in the blocks. When the energy of the block reaches the threshold value, it is released and transmitted to its closest neighbors. The released energy dissipates and radiates into the environment. If the neighboring block receives enough energy to exceed the threshold value, it also releases energy and this process takes the form of an avalanche, which, in fact, is a seismic event. The use of energy as a variable has an advantage since it is a scalar quantity. This makes it easy to apply a cellular automation scheme that formalizes the process of redistributing energy between blocks. In addition, energy is the main characteristic of most laws that describe a seismic process.

The hierarchical system is formed by blocks of five sizes (levels) with side sizes l_i, where l_i are integers. The smallest blocks have size $l_1 = 1$, and the size of the blocks of the next level is twice as large. The number of blocks of each level is chosen in such a way that the fractal dimension of the block medium is $D = 2.5$. Such a value of D is inherent in the distribution of fragments of most natural structured materials, that is, $N_i(>l_i) = C_i l_i^{-D}$, where N_i is the number of blocks of size greater than l_i [15]. In analogy with the classical cellular automation models [32,52], each block is in two states: in a state of rest (stable element) and in a disturbed state (unstable element). The block is considered to be stable if the energy accumulated by it is less than the threshold energy E_i^{th}. Otherwise, if the energy of the block reaches or exceeds the threshold value, $E_i \geqslant E_i^{\text{th}}$, then it loses its stability and reduces its energy. Unlike classic cellular automation models, the block loses only part of the stored energy during the unloading process, $E_i \to E_i^r = E_i^{\text{th}}\theta$, where the residual energy E_i^r is determined by the parameter θ. Since part of the energy dissipates and radiates in the form of seismic waves, the energy $(E_i - E_i^{\text{th}}\theta)(1 - \gamma\psi)$ is transferred to the neighboring blocks. Here $\psi \in [0,1]$ is a random number and γ is the coefficient determining the amount of dissipated and radiated energy. This energy is distributed between the adjacent blocks in proportion to the contact area,

$$E_k \longrightarrow E_k + \frac{\lambda_{ik} E_i^{\text{th}}}{S_i^2}\left(E_i - E_i^{\text{th}}\theta\right)(1 - \gamma\psi), \qquad (1)$$

where λ_{ik} is the area of contact between the ith and kth blocks and $S_i = 6l_i^2$. The threshold energy E_i^{th} depends on block size, namely, its surface area $E_i^{\text{th}} = S_i(1 + \delta_i)$. Here the symbol δ_i stands for the small noise obeying the Gaussian distribution with zero mean value and variance d_δ. Energy is injected into the block system discretely in portions $\Delta E = 1$ in one step at a time, just as in cellular automation models [32,40,41]. The probability of energy transfer is proportional to the surface area of the block. During the preparation and implementation of an earthquake, the fast and slow processes should be distinguished depending on speed: the former is associated with the energy transfer from tectonic plates into a seismic zone, and the latter is connected with an earthquake directly. Therefore, energy is transferred into the system during the slow process of elastic energy accumulation only, when earthquakes are absent.

To avoid the influence of boundary effects, all surfaces of area Ω are subjected to periodical conditions. In this case, the energy output is solely due to dissipation and seismic radiation. The simulation of the seismic process is carried out in the block system containing $n_5 = 50$ largest blocks and the total number $n_t = 62\,182$ providing the fractal dimension $D = 2.5$. At the beginning of the simulation, all blocks have a certain randomly distributed energy such that it does not exceed the threshold value in any block. After that the system shortly reaches a steady but nonequilibrium state with small fluctuations of total energy E_t, as it is shown in the inset of Fig. 2. Here, the temporal variation of total energy at four different values of coefficient θ, which regulates the residual energy E_i^r, is shown. It is evident that the system with the highest residual energy has the highest total energy.

Figure 2(a) shows the cumulative complementary distribution of earthquake radiated energy E_e for four values of coefficient θ. The straight line corresponds to the value of slope $\beta = 1.07 \pm 0.02$ for all values of residual energy; that is, the model reproduces accurately the GR law in the energy representation $N(>E) \propto E^{-\beta}$, in which the exponent varies in the range 0.80–1.05 [34]. The deviation from the power-law dependence caused by the limiting of block sizes occurs for large earthquakes. This is confirmed by the fact that the decreasing number of blocks leads to a greater bending of distribution functions [Fig. 2(a)]. Figure 2(b) shows the values of exponent β versus a lower energy cutoff E_e^*. In the graph it is easy to recognize the plateau, where β is almost constant and equals 1.17. From this it follows that the model supports the overvalued exponent β.

Seismic activity for different values of residual energy before and after major earthquakes indicates that there are no

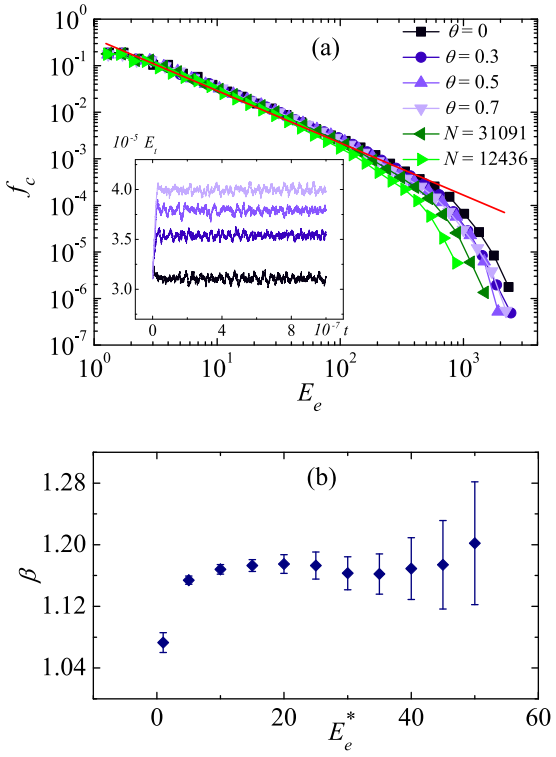

FIG. 2. The Gutenberg-Richter law. (a) The cumulative complementary distribution of events for different residual energies and different numbers of blocks. The slope of the linear fit to all four dependencies is 1.07. Inset: Time dependence of total system energy E_t for different θ. (b) The dependence of exponent β on a lower energy cutoff E_e^*; the error bars are 95% bootstrap confidence intervals.

series of aftershocks, although there are foreshocks [Fig. 3(a)]. Therefore, to describe the realistic seismic process possessing the aftershocks, this model should be improved. It is useful to utilize the conjecture that a large earthquake causes the significant destruction of rock massif and the redistribution of stresses in the excited area [9]. The destruction of rock results in the reduction of critical values of stresses (elastic energy)

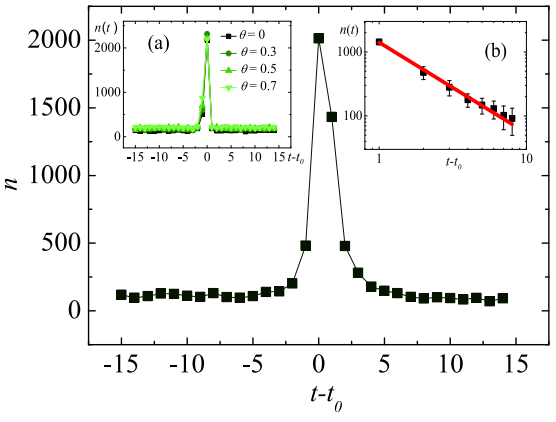

FIG. 3. The average earthquake occurrence versus that relative to mainshock occurrence times. (a) The model without improvement. (b) The power fit of aftershocks in the advanced model; error bars are 95% bootstrap confidence intervals.

that determine the conditions for the loss of equilibrium leading to the generation of aftershocks. In this model, the reduction of critical energy is described by the following procedure. In the area where an earthquake happened, at each time step each block randomly reduces the threshold

$$E_i^{\text{th}} \to \mu E_i^{\text{th}}(1+\epsilon_i), \tag{2}$$

where $\mu < 1$ is a constant, and ϵ_i denotes small noise with Gaussian distribution with zero mean value and the variation d_ϵ. The decreasing of E_i^{th} is applied until the threshold energy value reaches the residual energy $E_i^r = \theta S_i(1+\delta_i)$. After a significant interval of time, the regeneration ("rehabilitation") of destroyed connections occurs. This process also happens randomly when the condition $\chi_i \leqslant \varepsilon$ is fulfilled, where χ_i is a random variable generated for the ith block at every time step after a large earthquake, and ε is a small number providing the long time of rehabilitation. When the change of energy thresholds in the area covered by an earthquake takes place, then several aftershocks may be triggered simultaneously and all of them are taken into account for the construction of statistical dependencies.

The improved model demonstrates both foreshocks and aftershocks (Fig. 3). As in the previous model, large earthquakes are the earthquakes with energy exceeding the value $E^* = 1000$ and the total number of large earthquakes is $N = 843$. These data are obtained at fixed parameters $\mu = 0.6$, $d_\delta = 0.1$, $d_\epsilon = 0.1$, and $\varepsilon = 0.01$ and for four values of θ. The temporal attenuation of aftershock numbers of *n in situ* is known to obey the generalized Omori law

$$n(t) = k/(t+c)^p, \tag{3}$$

where the exponent p varies from 1.0 to 1.8, and c is a small quantity [8]. According to executed simulations, the temporal dependence of aftershocks is fitted by the curve with the coefficients $k = 1489$, $c = 0.03$, and $p = 1.50 \pm 0.04$ [Fig. 3(b)].

The parameter μ associated with a threshold reduction after a large earthquake (2) affects weakly the cumulative complementary distribution of earthquakes [Fig. 4(a)]. However, from Fig. 4(b) it follows that the influence of μ on $n(t)$ is significant. For values $\mu \geqslant 0.75$ this dependence breaks to be power. To study the relation between μ and p, Fig. 5 is plotted. Note that for $\mu < 0.75$ the constant p increases slightly from 1.17 to 1.56 with increasing μ.

The simulations confirm that the influence of noises δ_i and ϵ_i on $n(t)$ is not significant (Fig. 6). The exponent p does not practically change at different values of variances d_δ and d_ϵ. Similarly, the noises almost do not affect the exponent β. Reducing the critical energy to the value $E^* = 100$, the excess of which reduces the thresholds of E_i^{th}, practically does not affect either the exponent β or the exponent p.

Concerning aftershocks in a seismic process, there is another scaling law called the productivity law proposed by Utsu [8,9]. It describes the dependence of the total number N_a of aftershocks generated by an earthquake on its magnitude m_{ms},

$$N_a = N_0 \exp[\alpha(m_{\text{ms}} - m_0)], \tag{4}$$

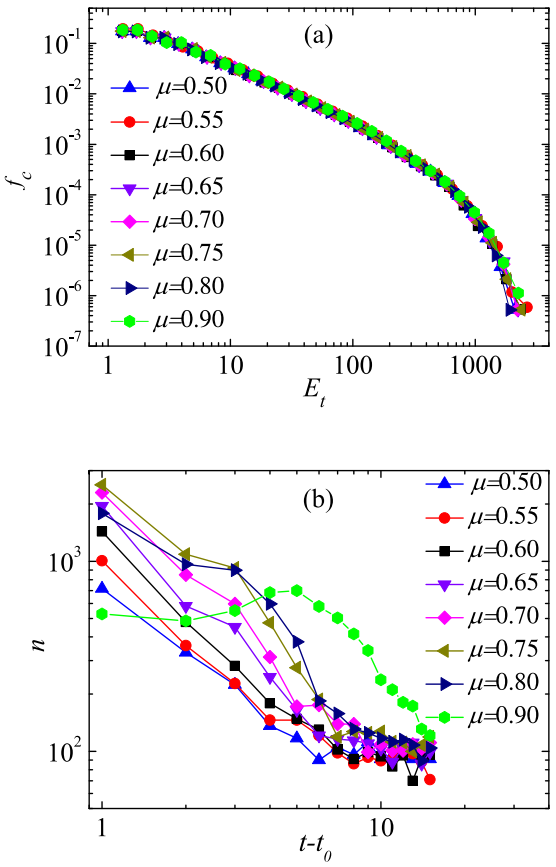

FIG. 4. (a) The cumulative complementary distribution of events and (b) the average number of aftershocks versus that relative to mainshock occurrence times for different μ.

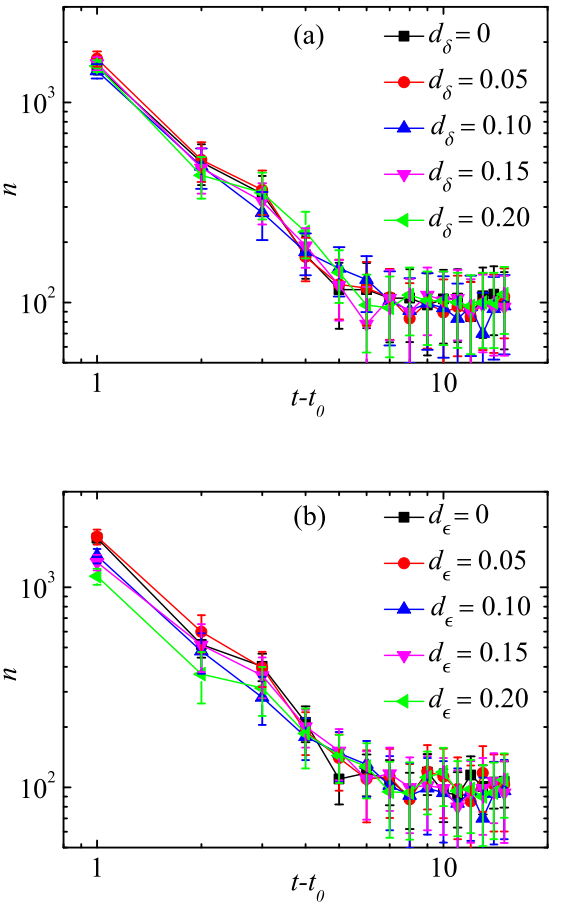

FIG. 6. The average aftershock occurrence versus that relative to mainshock occurrence times at different variances (a) d_δ and (b) d_ϵ. The error bars are 95% bootstrap confidence intervals.

where m_0 is the minimum magnitude cutoff and α is a constant. The transition from magnitude to energy gives

$$\log_{10} N_a = K \log_{10} E_{\rm ms} + C, \quad K, C = \text{const}. \tag{5}$$

As follows from Fig. 7 obtained at $\mu = 0.6$, $d_\delta = 0.1$, and $d_\epsilon = 0.1$, this dependence is almost linear in logarithmic coordinates with $K = 0.41 \pm 0.03$.

Another law regarding aftershocks, Båth's law, predicts that the difference in magnitude between a mainshock with magnitude $m_{\rm ms}$ and its largest detected aftershock with magnitude $m_{\rm as}^{\rm max}$,

$$\Delta m = m_{\rm ms} - m_{\rm as}^{\rm max}, \tag{6}$$

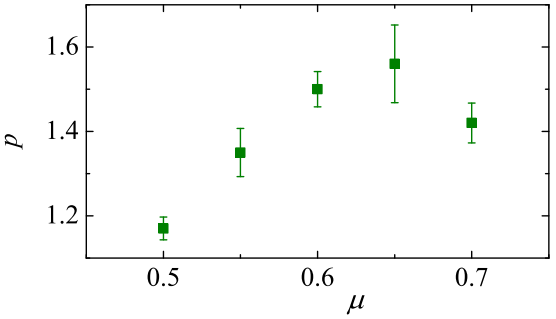

FIG. 5. Omori's law. The dependence of exponent p on the parameter μ with the error bars of 95% bootstrap confidence intervals.

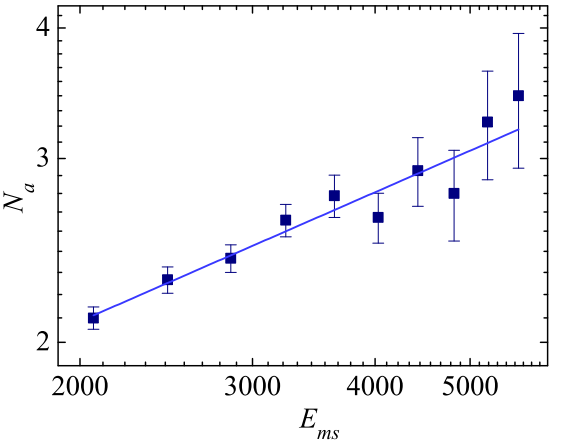

FIG. 7. The productivity law. Total number of aftershocks N_a versus energy $E_{\rm ms}$ of the main earthquake. The error bars are 95% bootstrap confidence intervals.

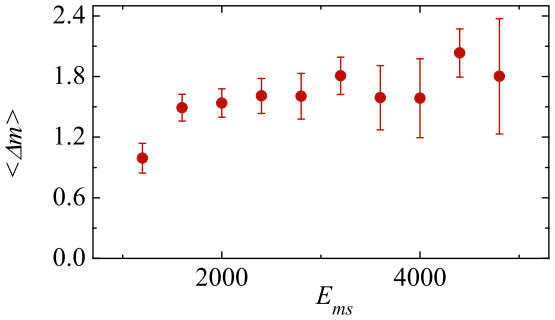

FIG. 8. Båth's law. The average value of the relative difference $\langle \Delta m \rangle$ in magnitude between the mainshock and its largest aftershock as a function of the mainshock energy $E_{\rm ms}$. The error bars are 95% bootstrap confidence intervals.

is close to 1.2, regardless of the mainshock magnitude [53,54]. In the energy representation this relation looks like

$$\Delta m = 1/A\big(\log_{10} E_{\rm ms} - \log_{10} E_{\rm as}^{\rm max}\big), \tag{7}$$

where $A = 1.5$. Figure 8 shows the dependence of the average value of the relative difference $\langle \Delta m \rangle$ on the main shock energy $E_{\rm ms}$. The relative difference $\langle \Delta m \rangle$ is close to a constant value and is slightly larger than the experimental one.

The hypocenters and epicenters of earthquakes form the fractal sets with the dimensions d_f^h and d_f^e in space and on the surface, respectively. According to numerous studies, the fractal dimension of earthquake epicenters varies from 1.0 to 1.8 [55,56], and the hypocentral dimension depends on the depth of earthquakes and falls from 2.2 for surface earthquakes to 1.5–1.6 for deep earthquakes [57,58]. In this model, the hypocenters were defined as the mean value for the positions of the centers of all cubes that were involved in the earthquake formation. The epicenters were defined in correspondence with their projections on the upper plane of the cube Ω. Figure 9 shows the spatial distribution of earthquake hypocenters, from

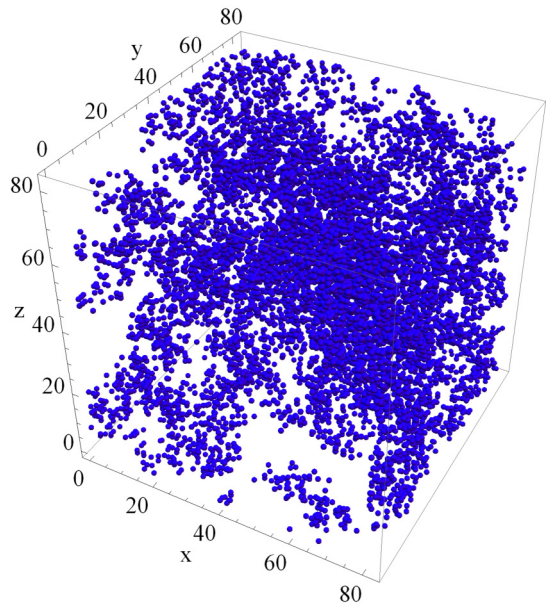

FIG. 9. The spatial distribution of hypocenters.

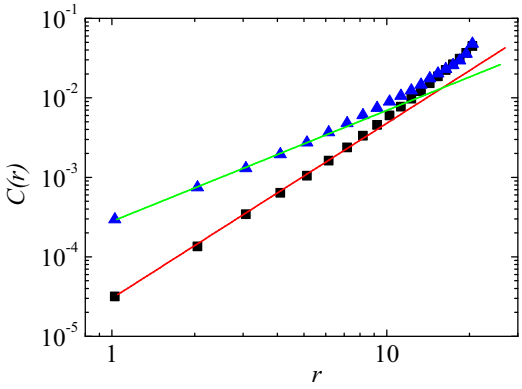

FIG. 10. Correlation integrals as the functions of the distances between hypocenters and epicenters in log-log coordinates and corresponding power-law fits.

which it is evident that the hypocenters are disposed irregularly and form clusters. The fractal dimensions d_f^h and d_f^e of the distribution are evaluated using the correlation integral method [59]. The correlation integral is defined as

$$C(r) = \lim_{N\to\infty} \frac{1}{N^2} \sum_{i,j} H(r - \mid \mathbf{r}_i - \mathbf{r}_j \mid), \tag{8}$$

where r is a distance, $\mathbf{r}_i$ and $\mathbf{r}_j$ are locations of hypocenters (epicenters) of the earthquakes i and j, and H is the Heaviside function. For fractal sets, the correlation integral $C(r) \propto r^{\upsilon}$, where the correlation exponent υ (known also as a two-point correlation dimension) is very close to the fractal dimension d_f. As a rule, to avoid the dependence $C(r)$ on N, the number of events, N, is chosen as large as possible. Here $N = 1\,176\,295$ and the resulting correlation integral dependencies on the distance for hypocenters and epicenters in double logarithmic coordinates are shown in Fig. 10. The calculated two-point correlation dimension for epicenters $\upsilon^e = 1.8$ falls into the interval of experimentally observed values. For hypocenters, $\upsilon^h = 2.8$ and slightly exceeds the fractal dimensions obtained for real earthquakes. This is due to the fact that in the model the area has the shape of a cube, whereas under natural conditions seismic zones are elongated along faults.

There is another approach for describing the temporal, spatial, and power properties of seismic processes developed by Bak *et al.* [56] and Corral [20–22], which uses the time between earthquakes with equal or greater magnitude, called waiting time or recurrence time. This approach is based on the existence of unified self-similar distribution for the waiting time τ: $P(\tau) = Rf(R\tau)$, where $f(x)$ is a scaling function and R is the rate of seismic activity. The function $f(x)$ is usually adjacent to the γ distribution:

$$f(x) \propto x^{\gamma-1} \exp(-x/\lambda) \tag{9}$$

with fitting parameters γ and λ. Figure 11 shows the distribution of waiting times after rescaling with the rate of seismic activity, R. The fitting function is the γ distribution (9) with the parameters $\gamma = 0.91 \pm 0.02$ and $\lambda = 1.12 \pm 0.04$. These parameters are less than those reported for earthquakes, $\gamma = 0.67 \pm 0.05$ and $\lambda = 1.58 \pm 0.15$ [21]. In this model the slow processes of accumulation and the rapid processes of energy

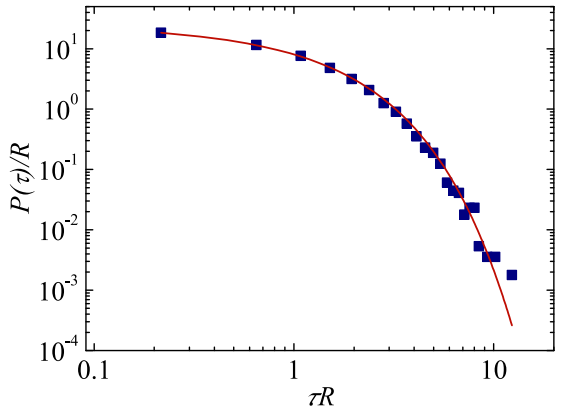

FIG. 11. The waiting time distribution rescaled by the rate of seismic activity, R. The solid fitting curve is the γ distribution (9) adjusted to the waiting time distribution via the least squares method.

relaxation proceed on the same temporal scale. In nature, unlike the model, the accumulation of elastic energy lasts for years or decades, and the release takes minutes. The simulation showed that increasing the duration of accumulated energy, that is, reducing the probability of bringing energy into the system, leads to an increase in the parameters γ and λ.

In summary, the developed hierarchical model incorporating the ideas of self-organized criticality and hierarchical structures reproduces the basic rules of seismic processes: the GR law with the exponent $\beta = 1.07 \pm 0.02$, Omori's law for aftershocks with the attenuation exponent $p = 1.50 \pm 0.04$, the availability of foreshocks, and the fractal properties of the spatial distribution of earthquakes with fractal dimensions $d_f^h \simeq 2.8$ and $d_f^e \simeq 1.8$ hypocenters and epicenters, respectively. This model gives a slightly large value of difference in magnitudes between a mainshock and the largest aftershock in comparison with real seismic processes. The waiting time distribution is well consistent with the γ distribution, but constants are smaller than real ones due to the fact that the model does not have a difference between temporal scales of accumulation and emission stages.

The simulation showed that all parameters in the model can be divided into two groups: parameters that significantly affect the behavior of the system and the parameters that have a weak effect on its behavior. The first group includes the parameters θ, γ, and μ and the second one includes d_δ, d_ϵ, and ε. Consequently, this model contains only three crucial parameters.

The advantage of this model is that there is no need to introduce auxiliary inhomogeneity to obtain a spatial fractal distribution of earthquakes, as has been made in the models mentioned above. The model takes into account already the natural hierarchical structure of a seismic area. Moreover, the description of the behavior of a seismic area after a strong earthquake is physically based. It should be also noted that several items remain beyond the discussion. This concerns the fact that the natural medium is a hierarchical system of embedded blocks rather than a system of randomly located blocks. In addition, the anisotropy of the seismic zone due to existing faults and morphological heterogeneity is not taken into account. In spite of these simplified conjectures, the model reproduces the main properties of seismic processes quite correctly.

This research is supported by the National Academy of Sciences of Ukraine, Grant No. 0113U000006.

[1] M. Alekseevskaya, A. M. Gabrielov, A. Gvishiani, A. Gelfand, and E. Ranzman, J. Geophys. **43**, 227 (1977).
[2] M. Sadovskiy, L. Bolhovitinov, and V. Pisarenko, Izv. Akad. Nauk SSSR, Fiz. Zemli **12**, 3 (1982) (in Russian).
[3] V. Keilis-Borok, Rev. Geophys. **28**, 19 (1990).
[4] *Nonlinear Dynamics of the Lithosphere and Earthquake Prediction*, edited by V. I. Keilis-Borok and A. A. Soloviev (Springer, Berlin, 2003).
[5] B. Gutenberg and C. Richter, *Seismicity of the Earth and Associated Phenomena*, 2nd ed. (Princeton University Press, Princeton, NJ, 1954).
[6] F. Omori, J. Coll. Sci. Imp. Univ. Tokyo **7**, 111 (1894).
[7] T. Utsu, Geophys. Mag. **30**, 521 (1961).
[8] T. Utsu, J. Fac. Sci., Hokkaido Univ., Ser. 7 **3**, 129 (1969).
[9] T. Utsu, J. Fac. Sci., Hokkaido Univ., Ser. 7 **3**, 197 (1970).
[10] R. Shcherbakov, D. L. Turcotte, and J. B. Rundle, Geophys. Res. Lett. **31**, L11613 (2004).
[11] B. Bodri, Fractals **01**, 539 (1993).
[12] M. C. Robertson, C. G. Sammis, M. Sahimi, and A. J. Martin, J. Geophys. Res. **100**, 609 (1995).
[13] J. Davidsen and M. Paczuski, Phys. Rev. Lett. **94**, 048501 (2005).
[14] Á. Corral, Phys. Rev. Lett. **97**, 178501 (2006).
[15] D. L. Turcotte, *Fractals and Chaos in Geology and Geophysics* (Cambridge University Press, Cambridge, UK, 1997).
[16] K. Nanjo and H. Nagahama, Pure Appl. Geophys. **157**, 575 (2000).
[17] P. Shebalin, I. Zaliapin, and V. Keilis-Borok, Phys. Earth Planet. Inter. **122**, 241 (2000).
[18] G. Zöller, S. Hainzl, and J. Kurths, J. Geophys. Res. **106**, 2167 (2001).
[19] S. Hainzl and T. Fischer, J. Geophys. Res. **107**, ESE 5 (2002).
[20] Á. Corral, Phys. Rev. E **68**, 035102 (2003).
[21] Á. Corral, Physica A **340**, 590 (2004).
[22] Á. Corral, Phys. Rev. Lett. **92**, 108501 (2004).
[23] J. R. Holliday, J. B. Rundle, D. L. Turcotte, W. Klein, K. F. Tiampo, and A. Donnellan, Phys. Rev. Lett. **97**, 238501 (2006).
[24] R. Shcherbakov, J. Van Aalsburg, J. B. Rundle, and D. L. Turcotte, Tectonophysics **413**, 53 (2006).
[25] P. Diodati, F. Marchesoni, and S. Piazza, Phys. Rev. Lett. **67**, 2239 (1991).
[26] J. P. Sethna, K. A. Dahmen, and C. R. Myers, Nature (London) **410**, 242 (2001).
[27] E. K. Salje and K. A. Dahmen, Annu. Rev. Condens. Matter Phys. **5**, 233 (2014).

[28] T. Mäkinen, A. Miksic, M. Ovaska, and M. J. Alava, Phys. Rev. Lett. **115**, 055501 (2015).
[29] H. V. Ribeiro, L. S. Costa, L. G. A. Alves, P. A. Santoro, S. Picoli, E. K. Lenzi, and R. S. Mendes, Phys. Rev. Lett. **115**, 025503 (2015).
[30] P. Bak, C. Tang, and K. Wiesenfeld, Phys. Rev. Lett. **59**, 381 (1987).
[31] P. Bak, C. Tang, and K. Wiesenfeld, Phys. Rev. A **38**, 364 (1988).
[32] P. Bak and C. Tang, J. Geophys. Res. **94**, 15635 (1989).
[33] K. Ito and M. Matsuzaki, J. Geophys. Res. **95**, 6853 (1990).
[34] Z. Olami, H. J. S. Feder, and K. Christensen, Phys. Rev. Lett. **68**, 1244 (1992).
[35] H. J. Jensen, *Self-Organized Criticality* (Cambridge University Press, Cambridge, UK, 1998).
[36] S. Hergarten and H. J. Neugebauer, Phys. Rev. Lett. **88**, 238501 (2002).
[37] R. Burridge and L. Knopoff, Bull. Seismol. Soc. Am. **57**, 341 (1967).
[38] J. B. Rundle and D. D. Jackson, Bull. Seismol. Soc. Am. **67**, 1363 (1977).
[39] S. R. Brown, C. H. Scholz, and J. B. Rundle, Geophys. Res. Lett. **18**, 215 (1991).
[40] B. Barriere and D. L. Turcotte, Geophys. Res. Lett. **18**, 2011 (1991).
[41] B. Barriere and D. L. Turcotte, Phys. Rev. E **49**, 1151 (1994).
[42] Y. Huang, H. Saleur, C. Sammis, and D. Sornette, Europhys. Lett. **41**, 43 (1998).
[43] M. Baiesi, Nonlinear Proc. Geophys. **16**, 233 (2009).
[44] H. Ceva, Phys. Rev. E **52**, 154 (1995).
[45] N. Mousseau, Phys. Rev. Lett. **77**, 968 (1996).
[46] M. Bach, F. Wissel, and B. Drossel, Phys. Rev. E **77**, 067101 (2008).
[47] C. A. Serino, K. F. Tiampo, and W. Klein, Phys. Rev. Lett. **106**, 108501 (2011).
[48] R. Dominguez, K. Tiampo, C. A. Serino, and W. Klein, Phys. Rev. E **87**, 022809 (2013).
[49] J. Kazemian, K. F. Tiampo, W. Klein, and R. Dominguez, Phys. Rev. Lett. **114**, 088501 (2015).
[50] O. Ramos, E. Altshuler, and K. J. Måløy, Phys. Rev. Lett. **96**, 098501 (2006).
[51] E. A. Jagla, Phys. Rev. E **81**, 046117 (2010).
[52] S. S. Manna, J. Stat. Phys. **59**, 509 (1990).
[53] M. Båth, Tectonophysics **2**, 483 (1965).
[54] A. Helmstetter and D. Sornette, Geophys. Res. Lett. **30**, 1 (2003).
[55] Y. Y. Kagan and L. Knopoff, Geophys. J. Int. **62**, 303 (1980).
[56] P. Bak, K. Christensen, L. Danon, and T. Scanlon, Phys. Rev. Lett. **88**, 178501 (2002).
[57] D. Harte, J. Nonlinear Sci. **8**, 581 (1998).
[58] Y. Y. Kagan, Geophys. J. Int. **168**, 1175 (2007).
[59] P. Grassberger and I. Procaccia, Physica D **9**, 189 (1983).